Materials Science & Engineering C 115 (2020) 111062

Contents lists available at ScienceDirect

Materials Science & Engineering C

journal homepage: www.elsevier.com/locate/msec

Functional behavior of chitosan/gelatin/silica-gentamicin coatings by electrophoretic deposition on surgical grade stainless steel

Tuba Aydemir[a], Liliana Liverani[a], Juan I. Pastore[b], Silvia M. Ceré[c], Wolfgang H. Goldmann[d], Aldo R. Boccaccini[a,*], Josefina Ballarre[a,c,**]

[a] Institute of Biomaterials, University of Erlangen-Nuremberg, 91058 Erlangen, Germany
[b] Digital Image Processing Lab.- ICyTe, CONICET-UNMdP, Juan B. Justo 4302, 7600 Mar del Plata, Argentina
[c] Applied Electrochemistry Div.-INTEMA, CONICET-UNMdP, Colon 10850, 7600 Mar del Plata, Argentina
[d] Department of Physics, Biophysics Group, University of Erlangen-Nuremberg, 91052 Erlangen, Germany

ARTICLE INFO

Keywords:
Electrophoretic deposition
Chitosan
Gelatin
Silica-gentamicin nanoparticles
Prevention of infections
Stainless steel implants

ABSTRACT

Metals are used in several orthopedic applications as fixation elements for the stabilization of fractures or as prostheses. One of the most common orthopedic biomaterials in many developing countries is surgical grade stainless steel (SS). However, its use as permanent implant in orthopedic surgery is conditioned due to its limited corrosion resistance in physiological media, lack of osseointegration, and absence of antibacterial effect. The aim of this work is to generate a degradable coating with antibacterial properties for stainless steel to be used in implants/medical devices. The coating is composed of a biopolymer/silica-gentamicin nanoparticles composite obtained by electrophoretic deposition (EPD) on surgical grade stainless steel plates. The coating surface was characterized by microscopic examination, and in vitro performance was evaluated after immersion in phosphate-buffered saline (PBS) solution, simulated body fluid (SBF), and cell culture medium, to analyze coating degradation, antibiotics release, cell attachment (ST-2 stromal cells), and antibacterial (*Escherichia coli* and *Staphylococcus aureus*) properties. EPD coatings were uniform and covered homogeneously the surface of the SS substrate. Also the distribution of silica-gentamicin nanoparticles was homogeneous on the coated area. The degradation of the chitosan-gelatin coatings was evident after 7 days of immersion. The gentamicin release led to excellent antibacterial behavior at 24 h, meanwhile the cell proliferation (at 7 days culture) was not inhibited. The results show that the coating system exhibits promising behavior which could contribute to prevent hospital infections at early implantation times.

1. Introduction

Metals do not generally generate efficient natural bonding with bone tissue, and it is therefore necessary to produce a mechanical anchor. This anchoring may be done by cementation (cemented prosthesis) or by the creation of a surface that is capable of generating an active response of the bone tissue, inducing new bone formation on the prosthesis (non-cemented prostheses) [1,2]. The later type of implant is mainly used when it is necessary to preserve bone tissue in patients with high mobility as in young people. The development of implant materials should consider obtaining a suitable surface to achieve integration with the adjacent bone. Both surface chemistry and morphology can affect cell anchorage and growth on the implanted material, thus affecting the compatibility of the interface between the host tissue and the material [3]. Surface modification of materials used in implantology is one of the most effective approaches to improve the biomaterial performance [4], since the interaction of the biological environment with the surface of the implant in the early stages of osteogenesis is fundamental for the success or failure of the prosthesis [5].

A positive outcome of a permanent implant material depends on several factors such as implant design, patient's general health, and surgeon ability or expertise. The factor that materials science and engineering deals with is the implant itself. There are three main goals that must be achieved with metallic implants for fixation purposes: fast bone regeneration [6], avoidance of corrosion and metallic product release to the surrounding medium [7], and prevention of infections [8]. Regarding corrosion, stainless steel is widely used in temporary and permanent implants; however it is susceptible to suffer crevice and

* Correspondence to: Aldo R. Boccaccini, Institute of Biomaterials, University of Erlangen-Nuremberg, 91058 Erlangen, Germany
** Correspondence to: Josefina Ballarre, Applied Electrochemistry Div.-INTEMA, CONICET-UNMdP, Colon 10850, 7600 Mar del Plata, Argentina.
E-mail addresses: aldo.boccaccini@ww.uni-erlangen.de (A.R. Boccaccini), jballarre@fi.mdp.edu.ar (J. Ballarre).

https://doi.org/10.1016/j.msec.2020.111062
Received 1 November 2019; Received in revised form 18 March 2020; Accepted 5 May 2020
Available online 07 May 2020
0928-4931/ © 2020 Elsevier B.V. All rights reserved.

pitting corrosion in physiological media [9].

At the present time the use of stainless steel removable screws for bone or plate fixation is considered, especially in developing countries. The improvement of the implant surfaces is a key issue for the success of the surgical procedure and for prompt patient recovery. Several kinds of bioactive apatite derivate coatings have been proposed over the past 20 years for improving bone fixation [10]; however, for complex and corrodible surfaces such as screws, there are just a few attempts reported in literature [11]. The use of biopolymers has also been considered for metal implants coatings. Natural polymers such as chitosan and gelatin, which can be used alone or together as coating material, have been investigated since they have excellent biocompatibility, degradation, full natural origin (so called green coatings), and possible antibacterial properties [12,13]. Such biopolymers are capable to bond to several surfaces and can be used in combination with functionalised particles for different applications. Electrophoretic deposition (EPD) is a versatile coating method, being increasingly used to produce coatings at room temperature, allowing the processing of a broad spectrum of materials [14]. Fine powder or colloidal suspensions of different materials, including biopolymers like gelatin and chitosan, can be deposited by EPD [15–17]. By combining electrophoresis and deposition, this technique offers many advantages, being favorable for diverse bioactive coating systems [16,18,21]. EPD facilitates producing uniform, stable, and mechanically resistant coatings with variable thickness on different shaped substrates as well as on three-dimensional complex and porous structures [22–24].

The addition of antibacterial agents to the metallic surface should help the surgeon to guarantee the normal development of the bone healing, contributing to the success of the implant. In this context, nosocomial infections are the cause of 50% of permanent implant revisions, [25], which means that the patient has to be re-operated or carefully treated with prolonged doses of antibiotics. Application of coatings on implants that can avoid bacteria colonization as well as induce localized bone regeneration is the main objective of several studies being carried out by biomaterial laboratories worldwide [8]. To avoid bacterial colonization, the use of several antibacterial agents incorporated into coatings has been widely studied [26–31]. Systemic administration of antibiotics for infection prophylaxis or treatment is well known, but the required local drug levels are difficult to reach an infected implant. A commonly used antibiotic is gentamicin, suitable to prevent implant-related infections in a short time after surgery. Since silica-based nanomaterials and their synthesis processes are biocompatible, cost effective, easily to handle as well as scalable for industrial purposes, they are good candidates for developing functional coatings [32,33]. In the typical nanoparticle shape (spherical), silica is investigated as a promising carrier system for drug delivery [34]. For preventing or fighting nosocomial infections, several “model drugs” have been tested [27,31,35,36] using silica nanoparticles as carriers. The aim of these systems is to achieve local release and controlled time-release of the selected drug, without affecting the main function of the implant-surface interface.

The aim of this work is to develop and characterize a chitosan-gelatin electrophoretically deposited coating containing silica-gentamicin nanoparticles on surgical grade stainless steel, for potential use as intracorporeal implant material with bioactive and antibacterial properties.

2. Experimental section

2.1. Materials and coatings

The used substrate was stainless steel AISI 316 L (Atlantic Stainless Co. Inc., composition: C 0.03% max, Mn 2% max, Si 1% max, P 0.045% max, S 0.03% max, Ni 10–14%, Cr 16–18%, Mo 2–3%). Rectangular sheets of 2.5 × 2 cm^2 and round samples of 1.5 cm diameter were used as substrates. The thickness of the substrates was 0.2 cm. The surface finishing was *as - received*. Samples were degreased, hand washed with distilled water, and rinsed with isopropanol previous to coatings deposition.

The components of the proposed coatings were two biopolymeric solutions (chitosan and gelatin) and silica-gentamicin nanoparticles. The first solution was prepared by dissolving 0.5 g of chitosan (medium molecular weight, deacetylation degree of 75–85% Sigma Aldrich) in 0.2 L deionized water and 10 mL acetic acid (VWR International, 99%). Then 0.79 L of ethanol (VWR International, 99–100%) was added, and the solution was stirred magnetically at room temperature for 24 h. To obtain the other solution, 1 g of gelatin type B (Sigma Aldrich) was mixed with 0.2 L of deionized water and 10 mL of acetic acid at 45 °C for 1 h. Then the solution was cooled down to room temperature, 0.79 L of ethanol was added and the solution was stirred. For preparing the final solution, equal amounts in volume of each separated solutions were used, with the aim of having 33 wt% chitosan and 67 wt% gelatin as final composition. This composition had been optimized in previous works [37,38].

Silica-gentamicin nanoparticles (labelled as SiGe NPs) were synthetized by a modified Stöber method [31]. Briefly, 75 mL ethanol (VWR International, 96%) was mixed with 3.4 mL of 25% w/vol ammonia solution (EMPROVE® Merck). 0.02 g of gentamicin sulfate (Sigma Aldrich) was incorporated, and the solution was stirred at room temperature for 1 h. 0.2 mL of tetraethoxysilane (TEOS, Sigma Aldrich® 99%) was dropped into the solution with vigorous stirring for 1 h, and then the suspension was stirred at room temperature for 24 h to complete the generation of nanoparticles. The obtained suspension was washed several times with distilled water to remove the remaining ammonia residual and finally the particles were freeze-dried. 2 g/L of the obtained SiGe NPs were added to the biopolymeric solutions.

The electrophoretically deposited coatings were obtained using direct current (DC) with an EX735M Multi-Mode PSU 75 V/150 V 300 W power supply (Thurlby Thandar Instruments Ld.). The SS 316 L substrates were used as cathode and also planar sheets of AISI 316 L stainless steel (ThyssenKrupp AG) were used as counter electrode. The surface condition of the SS samples was *as - received*, with a polished surface similar to 2,000 grit paper. The distance between electrodes was fixed at 10 mm, with a volume of 40 mL of suspension used for EPD. The trial and error principle was used to optimize the parameters for electrophoretic deposition. By using the Hamaker's model [39], the relationship between the parameters and the resulting deposition yield can be approximately evaluated. Thus, changes of deposition time and applied voltages formed the basis for the adaptation of the EPD process to obtain homogeneous and reproducible coatings. Finally, the deposition process was conducted by applying a constant voltage of 18 V for 5 min, at room temperature. Produced samples were air-dried and stored for further characterization.

2.2. Characterization methods

Particle size and its distribution are important characteristics determining the properties of composite materials, especially if this second (particulate) phase is composed of functional particles. To calculate size distribution of SiGe NPs images were acquired with Scanning Electron Microscopy (SEM) (Auriga Base ZEISS, Carl Zeiss Microscopy) with 1 kV accelerating voltage and Transmission Electron Microscopy (TEM) (JEM-2100F, Japan) operating at 94 kV. In this work, Digital Image Processing (DIP) was used to analyze the shape and distribution of the obtained nanoparticles, with an automatic algorithm described by Meng et al. [40]. This algorithm is mainly based on local adaptive Canny-edge detection, and it modifies circular Hough transform. For each spherical particle, the algorithm describes them using a single number —the diameter— because every dimension is identical. With this information, the particle size distribution is defined as the discrete function $p(d_k) = n_k$, where d_k is the *k*th diameter measured and n_k is the number of particles with that diameter. Particle size

distribution was obtained from 4 to 6 SEM images taken at the same magnification. The geometric mean was calculated with around 350 nanoparticles counted.

In vitro immersion tests were carried out with the aim of determining coating degradation and hydroxyapatite deposition ability of the systems. For these tests Phosphate-Buffered Saline (PBS) and Simulated body fluid (SBF) solutions were used: the first one was used to investigate degradation of the coatings, and the second one with the aim of simulating the concentration of inorganic ions in blood plasma and to observe hydroxycarbonateapatite (HCAp) formation [41]. The volume of solution used was according to the ISO/FDIS 23317 norm. The immersion times were 1, 3, 7, and 14 days. Fourier Transformed Infrared spectroscopy (FTIR) (Shimadzu IRAffinity-1S, Shimadzu Corp., transmittance mode, range of 400–4000 cm^{-1} wavenumber and resolution of 4 cm^{-1}) and X Ray Diffraction (XRD) (MiniFlex 600, Rigaku, with Cu–Kα radiation at 40 kV and 15 mA) tests were conducted on previously immersed samples in SBF. After the immersion, FTIR and XRD measurements were performed on the generated surfaces at each time-point. Also, the morphology and integrity of the obtained coatings were analyzed by SEM before and after soaking in the solutions.

Gentamicin release from the coatings in vitro in PBS was analyzed by using an UV-VIS Spectrometer (Specord40 by Analytik Jena) with the software WinASPECT 2.5.8.0, and enhancing the antibiotic signal with Ninhydrin (Sigma Aldrich™), measuring absorption at 400 nm wavelength. For the measurement of the drug release, each coating condition was immersed by triplicate in 5 mL of PBS (Sigma AldrichTM) and was incubated at 37 °C for 30 min, 1 h, 2 h, 4 h, 8 h, 24 h, 48 h, 5, 8, 14, and 21 days. At each time-point, 1 mL of the sample solution was withdrawn, while the same amount was replaced by fresh PBS. Together with 0.3 mL of a ninhydrin stock-solution (2 mg/mL PBS), the aliquot was heated up to 95 °C in a water bath for 15 min, following known protocols [42,43]. After cooling down the spectrometric scan was executed. The cumulative concentration of the drug was calculated by a calibration curve and taking into account the extraction of 1 mL of sample solution at each time point.

Assessments of the cell viability, proliferation, and morphology of bone murine stromal ST-2 cell line (Leibniz Institute DSMZ - German Collection of Microorganisms and Cell Cultures GmbH) on the coated SS substrates were performed. The samples were disinfected by one-hour UV-light irradiation placed into 12-multi-well plate at 50 cm distance from the lamp. ST-2 cell culture was carried out in RPMI 1640 medium (Thermo Fisher Scientific) with a 10% fetal bovine serum (Lonza) and 1% penicillin/streptomycin (Lonza), incubating the cells at 37 °C with 5% CO_2. The seeding of the cells on the coated samples was done with a 100 μL drop of cell suspension with an inoculum ratio of 1.5×10^5 cells/mL. Then the wells were filled with 2 mL RPMI medium. Cell viability after 1 day and 7 days was determined using the WST-8 assay ((2-(2-methoxy-4-nitrophenyl)-3-(4-nitrophenyl)-5-(2.4-disulfophenyl)-2H-tetrazolium, monosodium salt), Sigma). Also, fluorescence staining was performed. Briefly, rhodamine phalloidin and DAPI (ThermoFisher Scientific) were used to stain actin filaments and cell nuclei, respectively. The staining protocol started with immersion of the samples in a fixation solution constituted by 1,4-piperazine-diethansulfonic acid buffer, ethylene glycol tetraacetic acid, polyethylene glycol, paraformaldehyde, PBS and sodium hydroxide (all reagents from Sigma) and in permeabilization buffer based on Triton-X and sucrose in PBS. Afterwards, rhodamine phalloidin (8 μL/mL) and DAPI (1 μL/mL) were added to each well. A fluorescent microscope (Axio Scope A1, Zeiss) with 5, 10 and 20× was used.

In order to evaluate the antibacterial effect of the coatings, Gram-positive *S. aureus* and Gram-negative *E. coli* bacteria were chosen as bacterial strains. Halo inhibition (direct) and turbidity suspension (indirect) tests were used to study the antibacterial properties of the coatings. Briefly, bacterial suspension with an optical density (OD) of 0.015 (OD at 600 nm) was prepared in sterile lysogenic broth (Luria/Miller medium, Carl Roth, Germany) and grown in an incubator at 37 °C during 24 h. Fresh agar (LB Agar (Lennox), Lab M Ltd.) was placed into petri dishes, and they were uniformly coated with 20 μL of each bacteria suspension. The samples were inserted with the coated side in contact with the agar and incubated at 37 °C for one day: The halo inhibition zones around coated substrates were captured with a digital camera and were measured by the image processing software ImageJ [44]. For the turbidity measurements, samples were disinfected in 24-well plates under UV light exposure for 1 h. Each well was filled with 2 mL of LB-medium (Luria/Miller medium, Carl Roth, Germany) and each type of bacteria to reach a final concentration of 0.015 OD at 600 nm. Afterwards, the plates containing the samples were incubated at 37 °C for different periods of time (3, 6, 8, 24, 30, and 48 h). At these given time-points, aliquots of bacterial suspension were taken out, and their optical density was recorded.

3. Results and discussion

3.1. Particle and coating morphological evaluation

SiGe nanoparticle size distribution is a key parameter of relevance for the design of the present coating system, since the degradation and release of the active antibacterial drug depends, on how much of the surface reactive area is available to be in contact with the surrounding biological fluid. To obtain the size distribution of nanoparticles, SEM (Fig. 1a) and TEM images (Fig. 1(b)) have been widely used, but with manual or semi-automated measurement, using graphical processing software. Also statistical size distribution analysis from the SEM images is time-consuming and labor-intensive. In addition, results are not always reproducible, with great intra- and inter-user variability. On the other hand, image analysis by Digital image Processing (e.g. with self-made software) provides a very useful method for the measurement of the size distribution of granular materials.

With the proposed method, explained in the Experimental section, an efficient automatic segmentation for the generated nanoparticles can be achieved (Fig. 1(c)). With this information it is possible to quantify the diameter of each nanoparticle and define the particle size distribution. Results confirmed that the synthesis of the SiGe NPs gives spherical and well distributed particles. Two diameter sizes were found at the particle distribution: 150 and 199 nm with a standard deviation < 15%. Also the surface and structure of the analyzed particles were investigated more deeply by inspection of TEM images. Fig. 1(b) as well as Fig. 2 illustrate the absence of a core-shell structure, and also indicate the surface roughness of the obtained particles.

From the obtained images it is not possible to affirm that the SiGe NPs are porous or hollow. The hypothesis is that with the present synthesis method, amorphous silica-gentamicin composite nanoparticles were created, where the drug is embedded in the volume of the particle, but exhibiting a radial distribution [45]. The negatively charged silanol groups from the silica precursor react with the positively charged gentamicin particles, generating the composite NPs [31].

The stability of the mixture of the two polymeric solutions is essential for a high quality electrophoretic deposition (EPD). Unstable solutions cannot provide the mobility of particles and hence their deposition on the electrode. The isoelectric point (IP) is the point, at which the overall charge of the suspension is zero (a neutral charge) [46]. The IP of chitosan is 6.2 [39], and the one of gelatin Type B is 4.8 [12]. In this work, the experimental procedure guarantees that the chitosan is deacetylated and hydrolyzed due to the acidic medium, when dissolving ensuring that in this process, $–COO^-$ groups are being formed. At low pH range, below their IP and pKa values, chitosan and gelatin are soluble, positively charged and able to form a colloidal polyelectrolyte complex (PEC). The intermolecular attractive forces between the $–COO^-$ groups of gelatin and the $-NH_3^+$ groups of chitosan, the electrostatic repulsion forces between the positively charged molecules and also hydrogen bonding guarantee the stability of this complex [47,48]. According to literature, bare silica nanoparticles

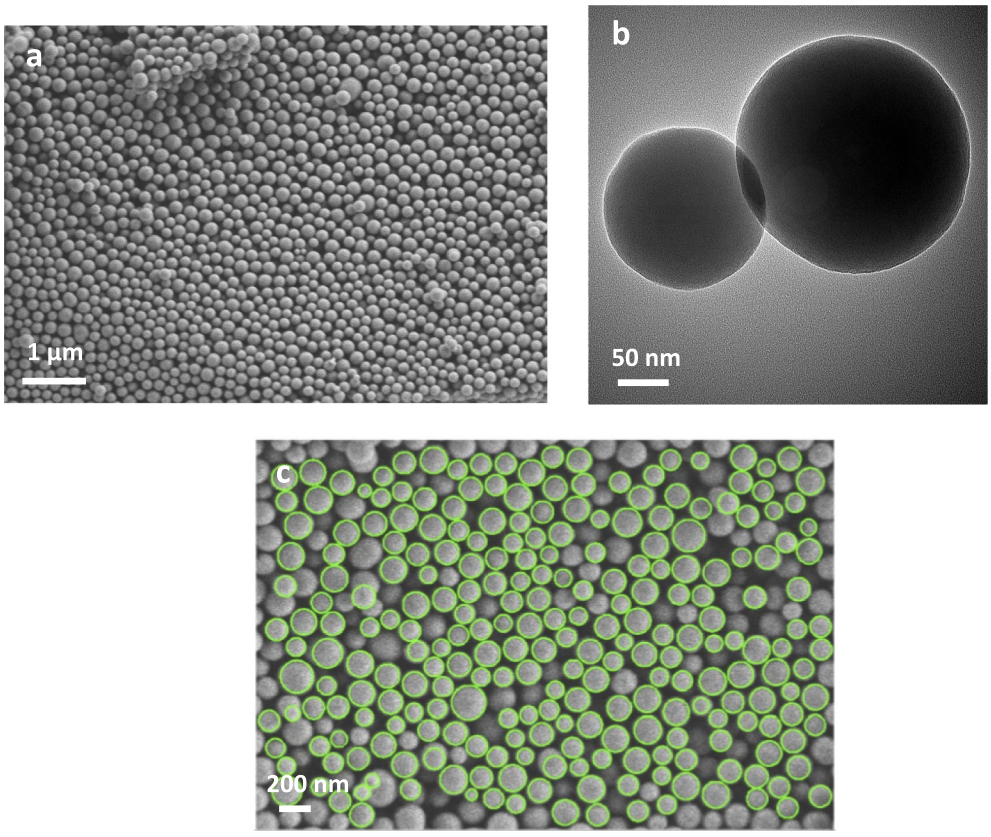


Fig. 1. (a) Scanning Electron Microscopy (SEM) image of the produced silica-gentamicin particles. (b) Transmission Electron Microscopy (TEM) image of the silica-gentamicin nanoparticles. (c) SEM image of the analyzed particles with the applied proposed image processing method.

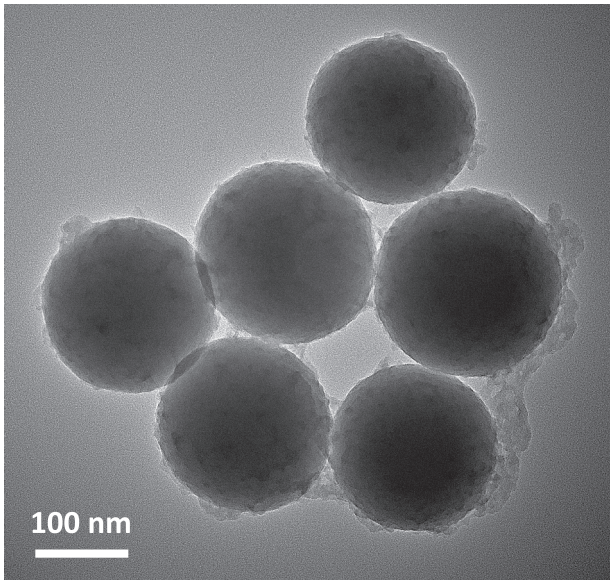


Fig. 2. Transmission Electron Microscopy image showing the surface of the silica-gentamicin nanoparticles.

typically have an IP around 2.8 [20]. Researchers also report that silanols can exist in three different forms on the silica surface, such as $SiOH^+$, SiOH and SiO^- - groups, which affects the surface charge for given pH values [20,31]. Consequently, silica nanoparticles show negative charges for pH values higher than 3. During the EPD process, the pH range of the solution is kept constant in the range between 3.5 and 4. In solution, the positively charged colloidal PEC of chitosan and gelatin [48] interconnects with negatively charged drug-loaded silica nanoparticles by electrostatically attractive interactions. Finally, this leads to a multiple positively charged and intermolecular stabilized composite, which migrates to the cathode after applying an electrical field; chitosan becomes insoluble and is deposited on the electrode together with gelatin and silica nanohybrids (Fig. 3). Also in Fig. 3(c), the cross-section of the generated coating, indicating fairly homogeneous distribution of NPs, can be seen.

Since for these colloidal suspensions significantly high potentials were measured, in comparison to the basic mixture of chitosan and gelatin, the addition of nanoparticles likely leads to the increase of the suspension stability. Repulsive and attractive interactions between molecules and charges of chitosan and gelatin are not avoidable. According to Patel et al. [19], this kind of formed interactions between negatively charged components and the chitosan/gelatin PEC are so strong that particles are carried along with the PEC during the deposition procedure because of its high mobility.

As previously explained in the Experimental section, several concentrations of chitosan, gelatin, and two concentrations of SiGe NPs were tested. Based on the data available in literature and the homogeneity of the obtained coatings [37,38,45], 1 g/L of gelatin, 0.5 g/L of chitosan and 2 g/L of SiGe NPs were chosen to study in this paper. The optimization of the EPD parameters was also performed, as mentioned in the Experimental section, leading to EPD time and voltage values suitable for obtaining robust and uniform coatings on stainless steel substrates. Coating adhesion is of great importance in this kind of applications [49]. The present coatings exhibited good adhesion to the SS substrates when the deposition parameters were optimized according to previous work [37].

After 1 day of exposure of the EPD chitosan/gelatin/SiGe NPs coated samples to phosphate buffer solution, the degradation of the coating was evident from SEM analysis (Fig. 4(a)). Part of the SIGe NPs

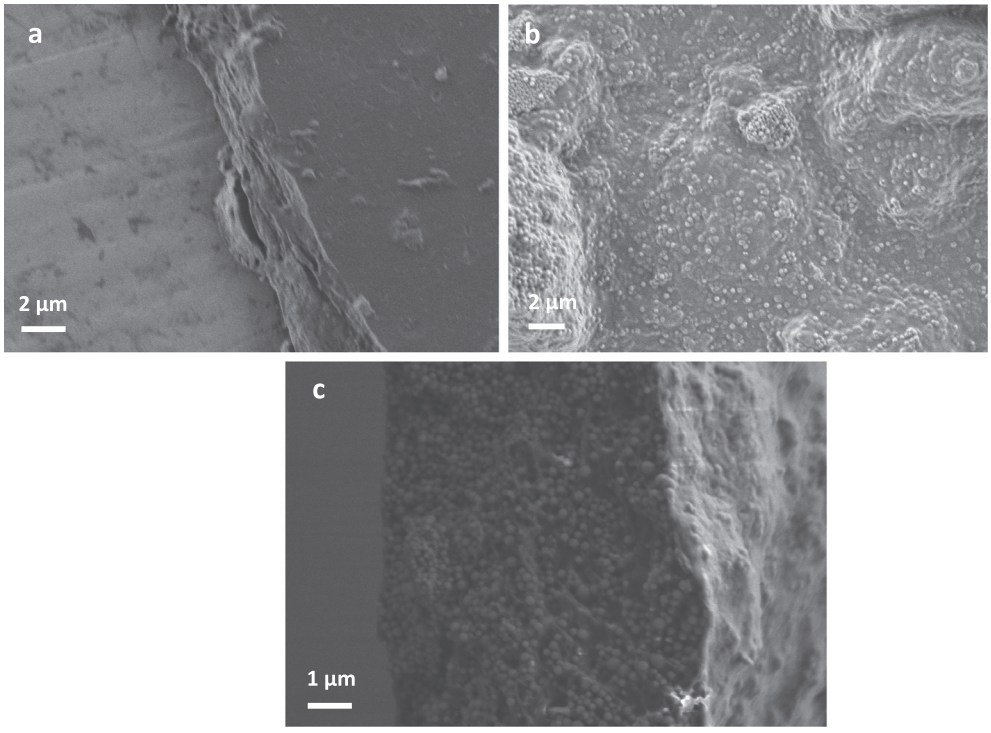


Fig. 3. (a) Scanning Electron Microscopy (SEM) image of the chitosan-gelatin coating on the stainless steel substrate. (b) SEM image of the chitosan-gelatin-silica gentamicin nanoparticle coating. (c) Cross-section SEM image of the chitosan-gelatin-silica gentamicin nanoparticle coating.

was released, and the ones that remained on the coating were seen to preserve their shape and size. After 21 days of immersion, the coating was much degraded and also most of the SiGe NPs were either released or degraded (Fig. 4(b)).

3.2. In vitro gentamicin release

Silica nanoparticles were selected as carriers for an antibacterial agent to obtain controllable drug release simultaneously with decomposition [34]. Therefore, this system should maintain an antibiotic release during a determined period of time in the area around the implant with a subsequent decay of the carrier. In this way, it would be possible to prevent bacterial adhesion and biofilm formation, if the amount of the antibiotic released reaches the Minimum Inhibitory Concentration (MIC) [50]. For *E. coli* and *S. aureus* the MIC values for gentamicin are between 1 and 4, and between 0.25 and 4 mg/L, respectively [51,52]. Thus, in this context, the release kinetics of gentamicin carried in the silica nanoparticles from a polymer containing matrix was studied. The cumulative gentamicin release curve obtained for the antibacterial coating is shown in Fig. 5. The obtained results for the chitosan/gelatin/SiGe NPs coating outline that the release kinetics of drug loaded

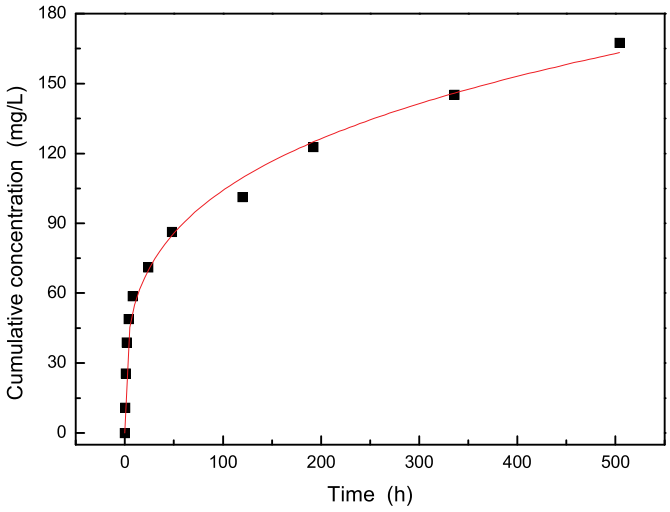


Fig. 5. Cumulative gentamicin release curve obtained for the EPD chitosan-gelatin- SiGe NPs coatings in PBS solution.

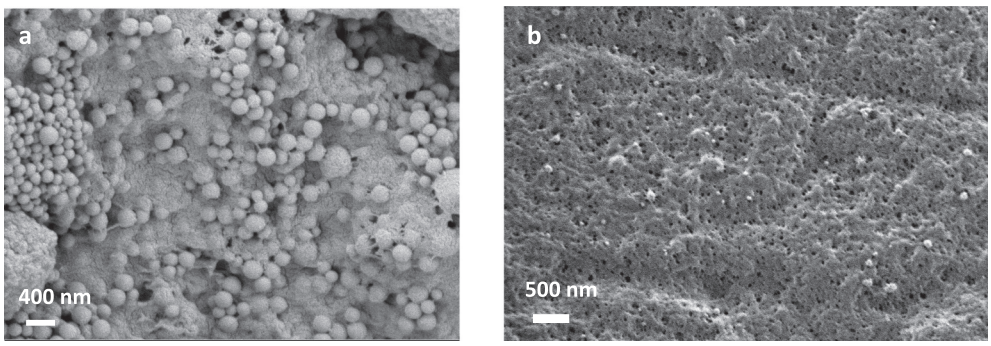


Fig. 4. Scanning Electron Microscopy (SEM) image of the chitosan/gelatin/SiGe NP- coating after immersion in PBS solution: (a) one day, and (b) 21 days.

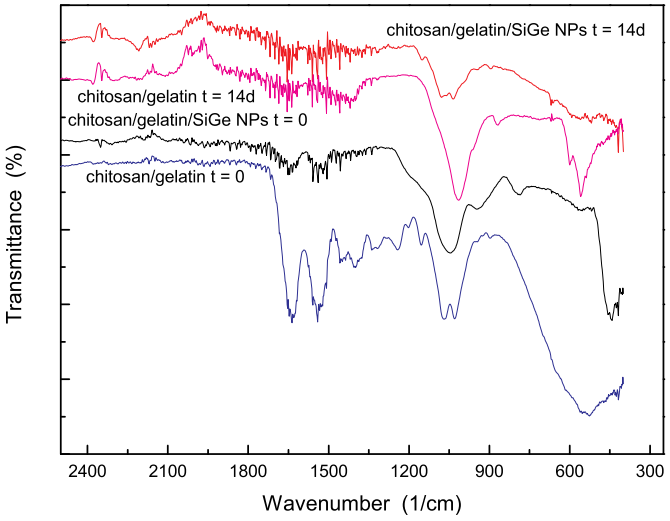


Fig. 6. Fourier Transform Infrared (FTIR) spectra for the SS samples with chitosan/gelatin EPD coating, and SS samples with chitosan/gelatin/SiGe NPs EPD coating, before and after immersion in SBF for 14 days.(The relevant peaks are discussed in the text).

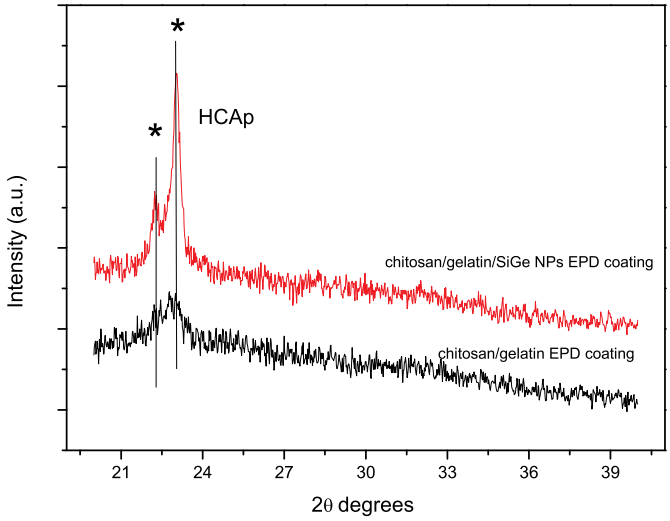


Fig. 7. X Ray Diffraction patterns of the chitosan/gelatin and chitosan/gelatin/SiGe NPs coatings after 14 days of immersion in SBF.

particles from the chitosan/gelatin matrix was controlled and influenced by their desired distribution inside and on the matrix. Additionally, this outcome supports the required SiO_2-carrier decomposition. These mentioned phenomena, together with the adequate degradation behavior of the coating, which was defined through different morphological and compositional factors, facilitated the sustained release of gentamicin within the 21 days of analysis. If the initial amount of gentamicin sulfate is considered to be the total amount of gentamicin in the SiGe NPs at the starting solution (192 mg/L), almost all the gentamicin is released at the end of the experiment (170 mg/L). It is relevant to notice that 40% of the gentamicin is released during the first 24 h of incubation, being an important hint for the prevention of bacterial biofilm formation at the early stage after implantation [53].

3.3. In vitro HCAp formation

Fig. 6 shows the degradation of the coating and formation of HCAp after immersion in SBF solution for 21 days. The main peaks in the FTIR spectrum of the gelatin-chitosan solution mixture used for EPD have small variations or changes from those of the main components alone. Although vibrations of some of the present components of the system may have overlapped with some new ones, some characteristic peaks are still able to be recognized. In all conditions studied, a broad band assigned to intermolecular electrostatic stability of the chitosan/gelatin PEC formed between $–COO^-$ and $-NH_3^+$ groups is noticed between 1530 cm^{-1} and 1678 cm^{-1} [54]. This band appears even after 14 days without showing a shift, which could be attributed to the remaining of the EPD coating on the surface after the immersion in SBF (Fig. 6). The broad band of chitosan centered at 1049 cm^{-1}, is also visible in all samples [54]. Before soaking in SBF solution, the spectrum corresponding to the composite coatings with chitosan/gelatin/SiGe NPs presents two sharp peaks in the range of 443 cm^{-1} and 1060 cm^{-1}. Both are associated to Si—O bonding in SiGe NPs, but the one at 1060 cm^{-1} is also associated to the chitosan and gelatin matrix. Also, two characteristic bands appeared at 800 cm^{-1} and 940 cm^{-1}, which correspond to symmetric stretching vibration of Si-O-Si [55]. After immersion, hydroxycarbonate apatite (HCAp) formation should be confirmed by showing the typical bands of phosphate (567, 603 and 1032 cm^{-1}) and carbonate (854 cm^{-1}, 1410 cm^{-1}) [56,57]. Some of the expected peaks are not clearly seen on the spectra, thus another method is needed to completely support and confirm the sample bioactivity in vitro.

With the aim to confirm the presence of HCAp, XRD measurements were also performed and results are shown in Fig. 7. The results refer to an immersion period of 14 days in SBF. To eliminate the metal background from the XRD pattern, the coatings and deposits after 14 days of immersion were scratched out to obtain a powder. In both types of coating (chitosan/gelatin and chitosan/gelatin with SiGe NPs coatings), characteristic peaks for deposited HCAp at around $2\theta = 23^\circ$ were found [58]; however, the main peak at $2\theta = 32^\circ$ is missing, which could be due to both the small amount of HCAp generated on the surface and the overlapping with the chitosan and gelatin peaks [2]. Also the low intensity of the peaks could be related with the low degree of crystallization of HCA, which is expected in early stages of bioactivity.

SEM images of the chitosan/gelatin/SiGe NPs coating on SS after 14 days of immersion in SBF are shown in Fig. 8. The typical needle-like and globular structure of the HCAp is observed.

3.4. In vitro cell behavior

The cell viability was measured by using the WST-8 assay after 1 day and 7 days for both type of coatings analyzed, and the bare stainless steel substrate was used as control (Fig. 8). Cells cultured without any substrate were used as positive control, too. It is noticeable that the three groups of analyzed samples were supportive for the proliferation of the bone murine stromal cells (ST-2 cells) after 7 days. SS samples promoted the adhesion, growth, and proliferation of cells for the two periods of time measured as well as the cells used as positive control. Bare stainless steel samples reach even higher values of cell growth in optical density than the separately proliferated cell cultures that were used as control. In contrary, the viability of cells on the EPD/SiGe NPs coatings is remarkable low. This is ascribable to the coating degradation in the medium and the medium refreshing procedure, which could also induce the detachment of cells.

On the one hand, comparing the EPD coating on stainless steel substrate with the EPD/SiGe NPs coating, it is possible that gentamicin could have acted as a minor inhibitor for cell proliferation at early times by providing slightly adverse effects during its initial release. On the other hand, it is noticeable that after 7 days, the viability of cells in presence of gentamicin reaches almost half of the value of the control cell culture. This indicates that at the beginning, the cell proliferation was probably impaired due to the initial burst release of gentamicin (within 24 h). The subsequent lower discharge might have facilitated a better cell growth and enlargement as confirmed by optical density

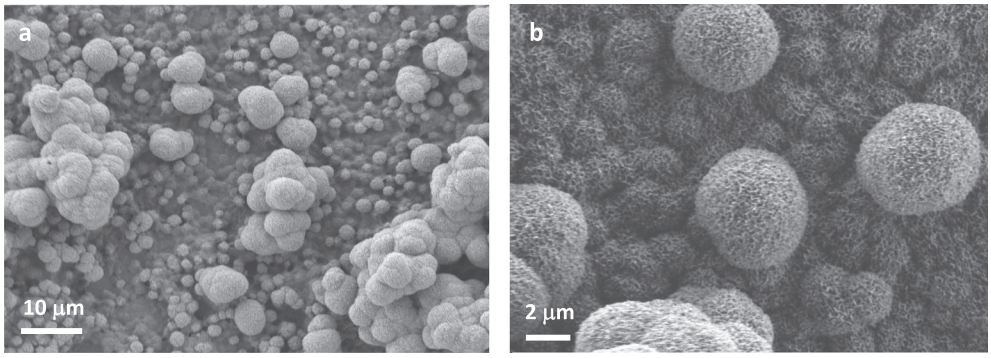


Fig. 8. Scanning Electron Microscopy (SEM) images at two magnifications of the chitosan-gelatin-silica gentamicin nanoparticle coating after 14 days of immersion in SBF solution, indicating formation of HCAp.

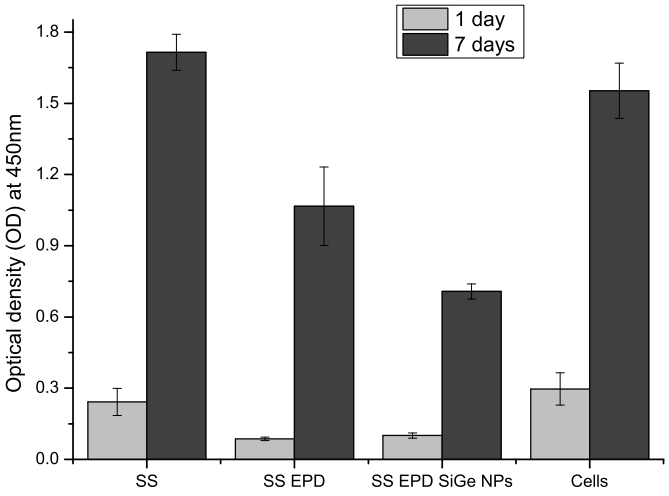


Fig. 9. WST-8 Cell viability tests for the bare, chitosan-gelatin EPD and chitosan-gelatin-SiGe NPs EPD coated stainless steel (SS) samples.

(OD) measurements. The ratio of cell proliferation and adhesion (OD 7 days/OD 1 day) gives a clearer idea about the cellular activity of the analyzed samples [59]. This ratio for the positive control (cells) was 5.2, while the ratio for the EPD coating without the SiGe NPs was 11.9, more than the double. It means that the chitosan and gelatin matrix is a suitable substrate for cell proliferation, even if at 7 days the coating starts to degrade. Both chitosan and gelatin biopolymers are known for their cell promotive properties. In particular gelatin contains distinct amino acids such as glycine, which can modulate cell adhesion [60]. The ratio for SS is 7.1, and the same ratio was found for the chitosan/gelatin/SiGe NPs coating, showing that the cell viability is relatively high, even in the presence of the SiGe NPs (Fig. 9).

Fluorescence microscopy images (Fig. 10), unlike the WST-8 assay, indicate that cells were well attached on both the chitosan/gelatin and the SiGe NPs coatings, but they were not easy to observe after 7 days to analyse cell proliferation. The artefacts of fluorescence in the samples after 7 days could be due to degradation or reaction of the chitosan/gelatin coating, or because cells are proliferating inside or under the coatings. A clear dispersion of the cells is evident since their nuclei are marked with the DAPI stain, where the blue dots in the picture represent individual cells.

Pishbin et al. [61] reported the non-toxicity of gentamicin towards osteoblast-like human osteosarcoma cells (MG-63). Since this behaviour is also shown in the present study, the slight inhibition effect with respect to the delay of cell proliferation during the initial release period of gentamicin should be investigated in more detail.

3.5. Antibacterial behavior

By direct contact to an agar medium, the inhibition capability of the coatings was preliminary investigated (Fig. 11) against gram positive (*S. aureus*) and gram negative (*E. coli*) bacteria. In comparison to the large inhibition areas created by the EPD chitosan/gelatin/SiGe NPs coatings, the bare metal and also the coatings with only chitosan/gelatin matrix were not successful to kill bacteria or to inhibit their growth: the diameters of the inhibition zone were 1.5 cm for bare SS (the diameter of the sample), 1.8 cm (*E. coli*) and 1.7 cm (*S. aureus*) for the chitosan/gelatin EPD coating, and 4.1 cm (*E. coli*) and 3.9 cm (*S. aureus*) for the chitosan/gelatin/SiGe NPs EPD coatings. Especially chitosan does not satisfy the expectation of antibacterial counteraction, although this is one of its usually mentioned specific properties [22,54]. Its low concentration in the present coatings (0.5 g/L) might have been determinative for the obtained results. Since the incubation of all samples was in a one day period, these results coincide with the drug release results shown above, and support the spectrometric initial results of around 40% of gentamycin release within 24 h.

Thus, turbidity measurements were carried out as an indirect method to analyze the antibacterial effect of the coatings. Due to the release of gentamicin and its counteraction capability in a bacterial suspension, changes in optical density occur, which were determined on different time points. The results regarding the measured values are presented in Fig. 12.

It can be noticed that both strains of bacteria grow with time and after 9 h they seem to grow very fast, assuming that they might be close to biofilm formation [62–65]. However, in the case of both gram-positive (*S. aureus*) and gram-negative (*E. coli*) bacteria with chitosan/gelatin/SiGe NPs stainless steel- coated samples, no bacterial growth was noticed, even after 30 h of immersion in the medium solution. This result supports the antibacterial early time inhibition behavior of the studied samples.

4. Conclusions

The present work introduced a novel and efficient drug delivery system incorporated into biodegradable coatings applied by EPD on metallic surfaces as stainless steel. The synthesized silica-gentamicin nanoparticles presented diameters < 200 nm and an amorphous structure that allow particle degradation and release of the drug. The effective release of antibiotics such as gentamicin was proven, and the

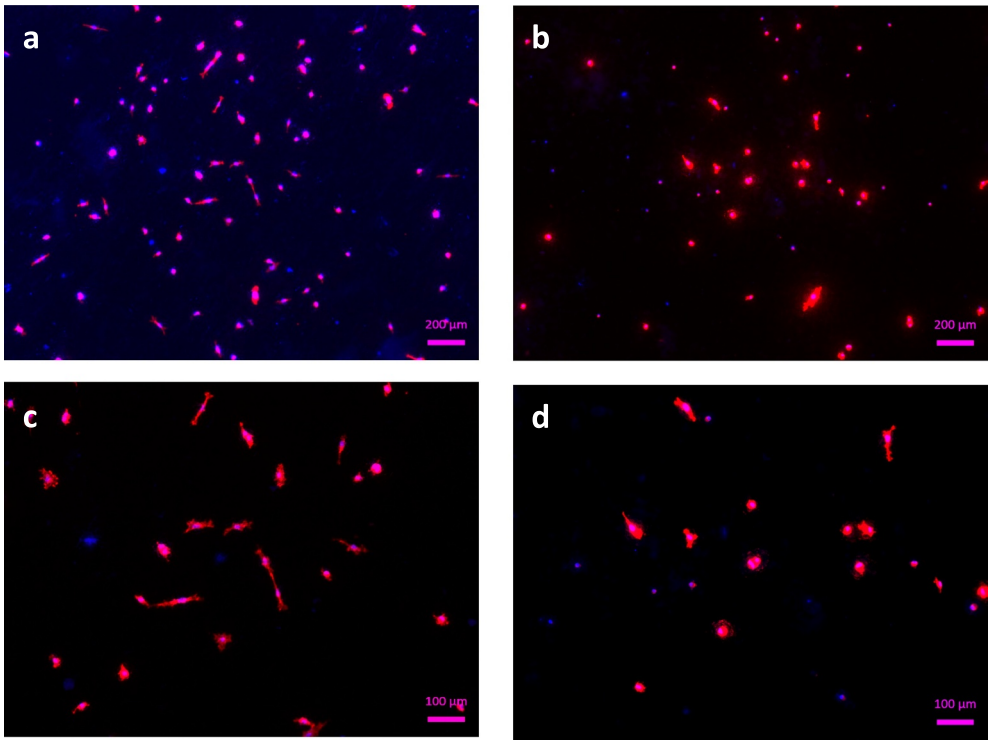


Fig. 10. Fluorescence microscopy images of cells over (a) SS chitosan-gelatin EPD coating with 100× magnification, (b) SS chitosan-gelatin-SiGe NPs EPD coating with 100× magnification, (c) SS chitosan-gelatin EPD coating with 200×, and (d) SS chitosan-gelatin-SiGe NPs EPD coating with 200×. In all images, the marking for nuclei is in blue and the cell cytoskeleton is in red. (For interpretation of the references to colour in this figure legend, the reader is referred to the web version of this article.)

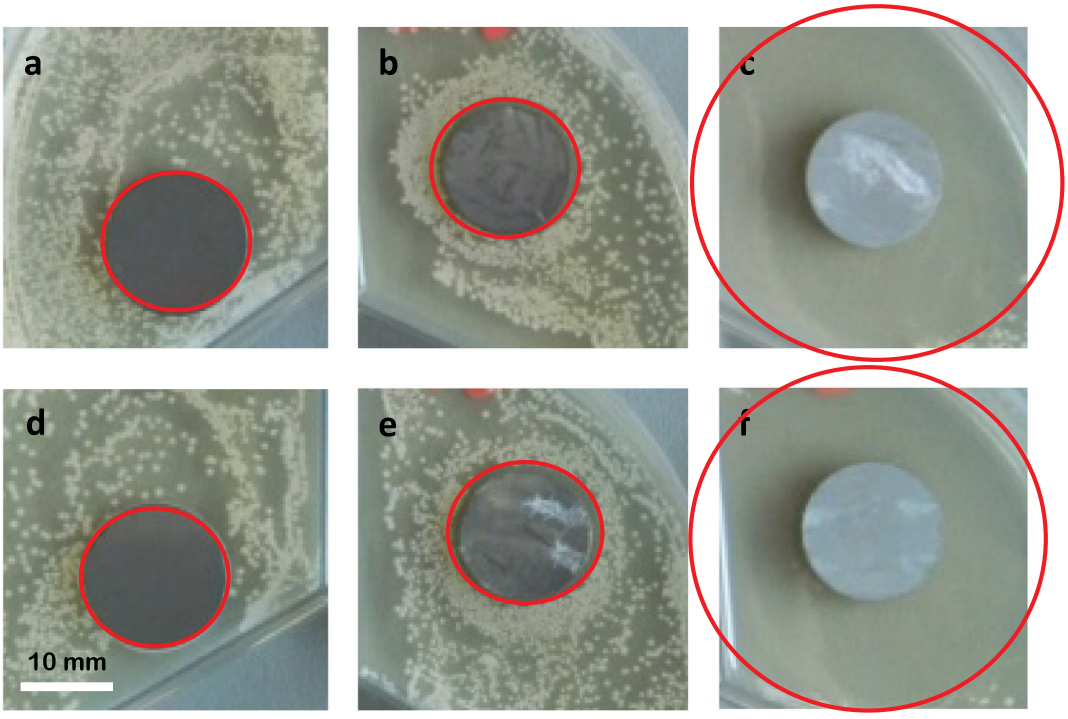


Fig. 11. Bacterial inhibition tests after 24 hs (direct contact, halo test) for: (a) bare SS sample with *S. aureus*, (b) chitosan-gelatin EPD coating on SS with *S. aureus*, (c) chitosan-gelatin-SiGe NPs EPD coating on SS with *S. aureus*, (d) bare SS sample with *E. coli*, (e) chitosan-gelatin EPD coating on SS with *E. coli*, and (f) chitosan-gelatin-SiGe NPs EPD coating on SS with *E. coli*. Inhibition zones marked with red circles in each case. (For interpretation of the references to colour in this figure legend, the reader is referred to the web version of this article.)

present approach could also be adapted for other drug release applications. Compact and flawless coatings were obtained, allowing the SiGe NPs dissolution as well as hydroxycarbonated apatite deposition, first insight of bioactivity. Positive results were obtained in terms of antibacterial properties combined with the fact that adhesion and proliferation of pre-osteoblastic cells were not inhibited. The gentamicin release was found to be higher than the minimum inhibition concentration, therefore the generation of resistant bacteria could be avoided. Further studies will be focused on investigating the mechanism of interaction between gentamicin and cells to elucidate the correct antibiotic concentration leading to improved cell attachment and by maintaining the antibacterial effect.

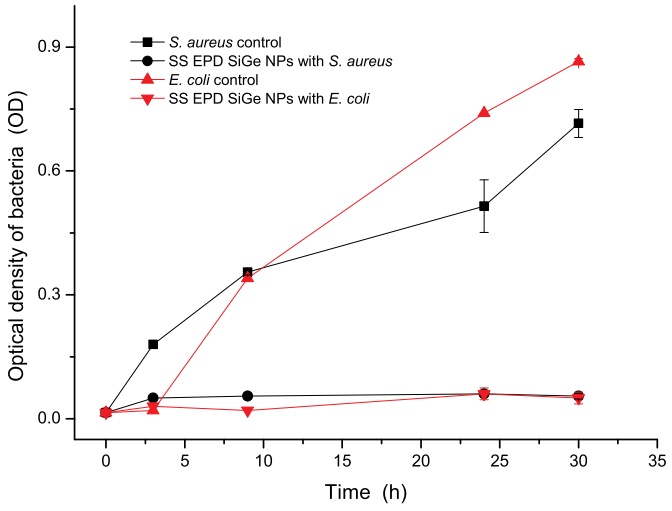


Fig. 12. Turbidity bacterial test (indirect test) plot with the optical density of different bacteria over time for the SS sample coated with chitosan-gelatin-SiGe NPs.

CRediT authorship contribution statement

Tuba Aydemir: Investigation, Validation.**Liliana Liverani:** Methodology, Investigation.**Juan I. Pastore:**Software, Formal analysis.**Silvia M. Cere:**Writing - review & editing.**Wolfgang H. Goldmann:**Validation, Writing - review & editing.**Aldo R. Boccaccini:**Supervision, Writing - review & editing, Conceptualization, Resources.**Josefina Ballarre:**Conceptualization, Methodology, Writing - original draft, Project administration.

Acknowledgements

The authors would like to acknowledge Dr. Maria Katunar, Dr. Agata Lapa for the support with the antibacterial tests, and Dr. Kai Zheng for the TEM images. The authors acknowledge funding from DFG (Deutsche Forschungsgemeinschaft, project Go598). Dr. Ballarre thanks the Alexander von Humboldt Foundation for the Georg Forster Fellowship to experienced researchers.

Declaration of competing interest

The authors declare that they have no known competing financial interests or personal relationships that could have appeared to influence the work reported in this paper.

References

[1] M. Niinomi, M. Nakai, J. Hieda, Development of new metallic alloys for biomedical applications, Acta Biomater. 8 (2012) 3888–3903.
[2] Q. Chen, G.A. Thouas, Metallic implant biomaterials, Materials Science and Engineering R: Reports 87 (2015) 1–57.
[3] M. Geetha, A.K. Singh, R. Asokamani, A.K. Gogia, Ti based biomaterials, the ultimate choice for orthopaedic implants - a review, Prog. Mater. Sci. 54 (2009) 397–425.
[4] S.R. Paital, N.B. Dahotre, Calcium phosphate coatings for bio-implant applications: materials, performance factors, and methodologies, Materials Science and Engineering R: Reports 66 (2009) 1–70.
[5] S. Bauer, P. Schmuki, K. von der Mark, J. Park, Engineering biocompatible implant surfaces: part I: materials and surfaces, Prog. Mater. Sci. 58 (2013) 261–326.
[6] J. Ballarre, Y. Liu, E. Mendoza, H. Schell, F. Díaz, J.C. Orellano, et al., Enhancing low cost stainless steel implants: bioactive silica-based sol-gel coatings with wollastonite particles, International Journal of Nano and Biomaterials 4 (2012) 33–53.
[7] J.J. Jacobs, M.D. Jeremy, J.L. Gilbert, R.M. Urban, Current concept review - corrosion of metal orthopaedic implants. The journal of bone & joint surgery, Incorporated 80 (1998) 268–282.
[8] A.G. Gristina, Biomaterial-centered infection: microbial adhesion versus tissue integration, Science 237 (1987) 1588–1595.
[9] D.A. López, A. Duran, S. Ceré, Electrochemical characterization of AISI 316L stainless steel in contact with simulated body fluid under infection conditions, J. Mater. Sci. Mater. Med. 19 (2008) 2137–2144.
[10] J.R. Jones, Review of bioactive glass: from Hench to hybrids, Acta Biomater. 9 (2013) 4457–4486.
[11] J. Hyup Lee, H.-S. Ryu, D.-S. Lee, K. Sun Hong, B.-S. Chang, C.-K. Lee, Biomechanical and histomorphometric study on the bone–screw interface of bioactive ceramic-coated titanium screws, Biomaterials 26 (2005) 3249–3257.
[12] A. Di Martino, M. Sittinger, M.V. Risbud, Chitosan: a versatile biopolymer for orthopaedic tissue-engineering, Biomaterials 26 (2005) 5983–5990.
[13] M. Jridi, S. Hajji, H.B. Ayed, I. Lassoued, A. Mbarek, M. Kammoun, et al., Physical, structural, antioxidant and antimicrobial properties of gelatin-chitosan composite edible films, Int. J. Biol. Macromol. 67 (2014) 373–379.
[14] I. Corni, M.P. Ryan, A.R. Boccaccini, Electrophoretic deposition: from traditional ceramics to nanotechnology, J. Eur. Ceram. Soc. 28 (2008) 1353–1367.
[15] F. Pishbin, V. Mouriño, J.B. Gilchrist, D.W. McComb, S. Kreppel, V. Salih, et al., Single-step electrochemical deposition of antimicrobial orthopaedic coatings based on a bioactive glass/chitosan/nano-silver composite system, Acta Biomater. 9 (2013) 7469–7479.
[16] F. Pishbin, A. Simchi, M.P. Ryan, A.R. Boccaccini, Electrophoretic deposition of chitosan/45S5 bioglass® composite coatings for orthopaedic applications, Surf. Coat. Technol. 205 (2011) 5260–5268.
[17] F. Gebhardt, S. Seuss, M.C. Turhan, H. Hornberger, S. Virtanen, A.R. Boccaccini, Characterization of electrophoretic chitosan coatings on stainless steel, Mater. Lett. 66 (2012) 302–304.
[18] S. Van Vlierberghe, G.J. Graulus, S.K. Samal, I. Van Nieuwenhove, P. Dubruel, Porous hydrogel biomedical foam scaffolds for tissue repair, Biomedical Foams for Tissue Engineering Applications (2014) 335–390.
[19] K.D. Patel, R.K. Singh, E.-J. Lee, C.-M. Han, J.-E. Won, J.C. Knowles, H.-W. Kim, Tailoring solubility and drug delivery release from electrophoretic deposited chitosan-gelatin films on titanium, Surf. Coat. Technol. 242 (2014) 232–236.
[20] J.P. Cloarec, C. Chevalier, J. Genest, J. Beauvais, H. Chamas, Y. Chevolot, et al., pH driven addressing of silicon nanowires onto Si3N4/SiO2 micro-patterned surfaces, Nanotechnology 27 (2016) 0957–4484.
[21] S. Perni, K. Martini-Gilching, P. Prokopovich, Controlling release kinetics of gentamicin from silica nano-carriers, Colloids Surf. A Physicochem. Eng. Asp. 541 (2018) 212–221.
[22] X.-Y. Wang, C.-S. Wang, M.-C. Heuzey, Complexation of chitosan and gelatin: from soluble complexes to colloidal gel, Int. J. Polym. Mater. Polym. Biomater. 65 (2016) 96–104.
[23] S.M. Ahsan, C.M. Rao, The role of surface charge in the desolvation process of gelatin: implications in nanoparticle synthesis and modulation of drug release, Int. J. Nanomedicine 12 (2017) 795–808.
[24] L.-Y. Huang, T.-Y. Liu, T.-Y. Liu, A. Mevold, A. Hardiansyah, H.-C. Liao, et al., Nanohybrid structure analysis and biomolecule release behavior of polysaccharide-CDHA drug carriers, Nanoscale Res. Lett. 8 (2013) 417.
[25] M. Diefenbeck, T. Mückley, G.O. Hofmann, Prophylaxis and treatment of implant-related infections by local application of antibiotics, Injury 37 (2006) S95–S104.
[26] S. Ahn, S. Lee, J. Kook, B. Lim, Experimental antimicrobial orthodontic adhesives using nanofillers and silver nanoparticles, Dent. Mater. 25 (2009) 206–213.
[27] L. Li, L. Wang, Y. Xu, L. Lv, Preparation of gentamicin-loaded electrospun coating on titanium implants and a study of their properties in vitro, Arch. Orthop. Trauma Surg. 132 (2012) 897–903.
[28] K. Subramani, R.T. Mathew, Titanium surface modification techniques for dental implants-from microscale to Nanoscale, Emerging Nanotechnologies in Dentistry, 2012, pp. 85–102.
[29] L. Zhang, J. Yan, Z. Yin, C. Tang, Y. Guo, D. Li, et al., Electrospun vancomycin-loaded coating on titanium implants for the prevention of implant-associated infections, Int. J. Nanomedicine 9 (2014) 3027–3036.
[30] H. Qin, Y. Zhao, Z. An, M. Cheng, Q. Wang, T. Cheng, et al., Enhanced antibacterial properties, biocompatibility, and corrosion resistance of degradable Mg-Nd-Zn-Zr alloy, Biomaterials 53 (2015) 211–220.
[31] A.M. Mebert, C. Aimé, G.S. Alvarez, Y. Shi, S.A. Flor, S.E. Lucangioli, et al., Silica core–shell particles for the dual delivery of gentamicin and rifamycin antibiotics, J. Mater. Chem. B 4 (2016) 3135–3144.
[32] X.-k. Ma, N.-H. Lee, H.-J. Oh, J.-W. Kim, C.-K. Rhee, K.-S. Park, et al., Surface modification and characterization of highly dispersed silica nanoparticles by a cationic surfactant, Colloids Surf. A Physicochem. Eng. Asp. 358 (2010) 172–176.
[33] M. Vallet-Regí, D. Arcos, Bioceramics for drug delivery, Acta Mater. 61 (2013) 890–911.
[34] G.S. Alvarez, C. Hélary, A.M. Mebert, X. Wang, T. Coradin, M.F. Desimone, Antibiotic-loaded silica nanoparticle–collagen composite hydrogels with prolonged antimicrobial activity for wound infection prevention, J. Mater. Chem. B 2 (2014) 4660–4670.
[35] P. Zhao, H. Liu, H. Deng, L. Xiao, C. Qin, Y. Du, et al., A study of chitosan hydrogel with embedded mesoporous silica nanoparticles loaded by ibuprofen as a dual stimuli-responsive drug release system for surface coating of titanium implants, Colloids Surf. B: Biointerfaces 123 (2014) 657–663.
[36] J. Wang, G. Wu, X. Liu, G. Sun, D. Li, H. Wei, A decomposable silica-based antibacterial coating for percutaneous titanium implant, Int. J. Nanomedicine 12 (2017) 371–379.
[37] M.A.U. Rehman, M.A. Munawar, D.W. Schubert, A.R. Boccaccini, Electrophoretic deposition of chitosan/gelatin/bioactive glass composite coatings on 316L stainless steel: a design of experiment study, Surf. Coat. Technol. 358 (2019) 976–986.
[38] E. Avcu, F.E. Baştan, H.Z. Abdullah, M.A.U. Rehman, Y.Y. Avcu, A.R. Boccaccini, Electrophoretic deposition of chitosan-based composite coatings for biomedical applications: a review, Prog. Mater. Sci. 103 (2019) 69–108.

[39] H.C. Hamaker, Formation of a deposit by electrophoresis, Trans. Faraday Soc. 35 (1940) 279–287.
[40] Y. Meng, Z. Zhang, H. Yin, T. Ma, Automatic detection of particle size distribution by image analysis based on local adaptive canny edge detection and modified circular Hough transform, Micron 106 (2018) 34–41.
[41] T. Kokubo, H. Takadama, How useful is SBF in predicting in vivo bone bioactivity? Biomaterials 27 (2006) 2907–2915.
[42] P. Frutos Cabanillas, E. Díez Peña, J.M. Barrales-Rienda, G. Frutos, Validation and in vitro characterization of antibiotic-loaded bone cement release, Int. J. Pharm. 209 (2000) 15–26.
[43] R. Dorati, A. DeTrizio, M. Spalla, R. Migliavacca, L. Pagani, S. Pisani, et al., Gentamicin sulfate PEG-PLGA/PLGA-H nanoparticles: screening design and antimicrobial effect evaluation toward clinic bacterial isolates, Nanomaterials 8 (2018).
[44] C.A. Schneider, W.S. Rasband, K.W. Eliceiri, NIH image to ImageJ: 25 years of image analysis, Nat. Methods 9 (7) (2012) 671–675 (PMID 22930834).
[45] S. Zhang, Z. Chu, C. Yin, C. Zhang, G. Lin, Q. Li, Controllable drug release and simultaneously carrier decomposition of SiO2-drug composite nanoparticles, J. Am. Chem. Soc. 135 (2013) 5709–5716.
[46] E.A. Vogler, Structure and reactivity of water at biomaterial surfaces, Adv. Colloid Interf. Sci. 74 (1998) 69–117.
[47] L. Besra, M. Liu, A review on fundamentals and applications of electrophoretic deposition (EPD), Prog. Mater. Sci. 52 (2007) 1–61.
[48] N.G. Voron'ko, S.R. Derkach, Y.A. Kuchina, N.I. Sokolan, The chitosan-gelatin (bio) polyelectrolyte complexes formation in an acidic medium, Carbohydr. Polym. 138 (2016) 265–272.
[49] X. Nie, A. Leyland, A. Matthews, Deposition of layered bioceramic hydroxyapatite/TiO2 coatings on titanium alloys using a hybrid technique of micro-arc oxidation and electrophoresis, Surf. Coat. Technol. 125 (2000) 407–414.
[50] R.D. Moore, P.S. Lietman, C.R. Smith, Clinical response to aminoglycoside therapy: importance of the ratio of peak concentration to minimal inhibitory concentration, J. Infect. Dis. 155 (1987) 93–99.
[51] J.M. Andrews, Determination of minimum inhibitory concentrations, J. Antimicrob. Chemother. 48 (2001) 5–16.
[52] M. Barber, P.M. Waterworth, Activity of gentamicin against Pseudomonas and hospital staphylococci, Br. Med. J. 1 (1966) 203–205.
[53] K. Anselme, P. Linez, M. Bigerelle, D. Le Maguer, A. Le Maguer, P. Hardouin, et al., The relative influence of the topography and chemistry of TiAl6V4 surfaces on osteoblastic cell behaviour, Biomaterials 21 (2000) 1567–1577.
[54] M. Rinaudo, Chitin and chitosan: properties and applications, Progress in Polymer Science (Oxford) 31 (2006) 603–632.
[55] D.A. Mosselhy, W. He, U. Hynönen, Y. Meng, P. Mohammadi, A. Palva, Q. Feng, S.P. Hannula, K. Nordström, M.B. Linder, Silica–gentamicin nanohybrids: combating antibiotic resistance, bacterial biofilms, and in vivo toxicity, Int. J. Nanomedicine 13 (2018) 7939–7957.
[56] J.M. Kanczler, R.O.C. Oreffo, Osteogenesis and angiogenesis: the potential for engineering bone, European Cells and Materials 15 (2008) 100–114.
[57] I. Rehman, W. Bonfield, Characterization of hydroxyapatite and carbonated apatite by photo acoustic FTIR spectroscopy, J. Mater. Sci. Mater. Med. 8 (1997) 1–4.
[58] A. Osaka, Y. Miura, K. Takeuchi, M. Asada, K. Takahashi, Calcium apatite prepared from calcium hydroxide and orthophosphoric acid, J. Mater. Sci. Mater. Med. 2 (1991) 51–55.
[59] L. Liverani, M.S. Killian, A.R. Boccaccini, Fibronectin functionalized electrospun fibers by using benign solvents: best way to achieve effective functionalization, Front. Bioeng. Biotechnol. 7 (2019) (2019) art 68.
[60] J.V. McArthur, R.C. Tuckfield, C. Baker-Austin, Antimicrobial textiles, Handb. Exp. Pharmacol. 211 (2012) 135–152.
[61] F. Pishbin, V. Mouriño, S. Flor, S. Kreppel, V. Salih, M.P. Ryan, A.R. Boccaccini, Electrophoretic deposition of gentamicin-loaded bioactive glass/chitosan composite coatings for orthopaedic implants, ACS Appl. Mater. Interfaces 6 (2014) 8796–8806.
[62] L. Gritsch, C. Lovell, W.H. Goldmann, A.R. Boccaccini, Do bioresorbable polyesters have antimicrobial properties? J. Mater. Sci. Mater. Med. 29 (2018).
[63] D.W. Jackson, J.W. Simecka, T. Romeo, Catabolite repression of < em > Escherichia coli < /em > biofilm formation, J. Bacteriol. 184 (2002) 3406–3410.
[64] J.-H. Park, J.-H. Lee, M.H. Cho, M. Herzberg, J. Lee, Acceleration of protease effect on Staphylococcus aureus biofilm dispersal, FEMS Microbiol. Lett. 335 (2012) 31–38.
[65] V. Antoci, C.S. Adams, J. Parvizi, H.M. Davidson, R.J. Composto, T.A. Freeman, et al., The inhibition of Staphylococcus epidermidis biofilm formation by vancomycin-modified titanium alloy and implications for the treatment of periprosthetic infection, Biomaterials 29 (2008) 4684–4690.